Soft Matter

Soft Matter

ARTICLE

Structural tailoring of hydrogen-bonded poly(acrylic acid)/poly(ethylene oxide) multilayer thin films for reduced gas permeability

Fangming Xiang,[a] Sarah M. Ward,[b] Tara M. Givens[a] and Jaime. C. Grunlan[*ab]

Hydrogen bonded poly(acrylic acid) (PAA)/poly(ethylene oxide) (PEO) layer-by-layer assemblies are highly elastomeric, but more permeable than ionically bonded thin films. In order to expand the use of hydrogen-bonded assemblies to applications that require better gas barrier, the effect of assembling pH on the oxygen permeability of PAA/PEO multilayer thin films was investigated. Altering the assembling pH leads to significant changes in phase morphology and bonding. The amount of intermolecular hydrogen bonding between PAA and PEO is found to increase with increasing pH due to reduction of COOH dimers between PAA chains. This improved bonding leads to smaller PEO domains and lower gas permeability. Further increasing pH beyond 2.75 results in higher oxygen permeability due to partial deprotonation of PAA. By setting the assembling pH at 2.75, the negative impacts of COOH dimer formation and PAA ionization on intermolecular hydrogen bonding can be minimized, leading to a 50% reduction in the oxygen permeability of the PAA/PEO thin film. A 20 bilayer coating reduces the oxygen transmission rate of a 1.58 mm natural rubber substrate by 20X. These unique nanocoatings provide the opportunity to impart gas barrier to elastomeric substrates without altering their mechanical behavior.

1. Introduction

Gas barrier is a key property for many applications, such as food packaging,[1-4] organic electronic device encapsulation,[5-7] and tire fabrication.[8-10] Among the choices for gas barrier materials, polymers are most commonly used due to light weight, low cost, ease of processing and formability.[1] In order to meet the demanding requirements of emerging gas barrier applications, significant research has been conducted to improve the gas barrier of polymers.[11-14] One of the most common practices involves adding clay into a polymer matrix to take advantage of the large aspect ratio and impermeable nature of the nano platelets.[15] Conventional polymer/clay composites, fabricated via mechanical mixing, rarely exceed more than an order of magnitude improvement in oxygen barrier due to random orientation and insufficient exfoliation of clay platelets.[16-18] Near-perfect platelet orientation and clay exfoliation were more recently achieved with layer-by-layer (LbL) assembly.[19-21] In this case, clay/polyelectrolyte thin films were deposited onto plastic substrates through complementary interactions (most typically electrostatic) between components.[22-24]

Polymer/clay thin films fabricated using LbL assembly exhibit oxygen permeability that is orders of magnitude below other gas barrier alternatives,[20, 25, 26] such as SiO_x and Al_2O_3. Varying components and/or parameters used during the assembling process allows the spacing between clay layers to be expanded, which has led to further improvements in gas barrier.[27-29] Despite being excellent oxygen barriers, polymer/clay multilayer thin films are very rigid due to the inherent stiffness of clay platelets and high clay loading (>70 wt%).[19, 26] These stiff multilayer assemblies crack easily when moderately stretched (10% strain),[8] leading to catastrophic loss of gas barrier. It is for this reason that multilayer thin films assembled without clay platelets are considered more suitable for gas barrier applications requiring the ability to withstand stretching.

Gas barrier of all-polymer multilayer thin films has been shown to be as good as clay/polymer assemblies. Undetectable oxygen transmission rate (OTR <0.005 cm^3/(m^2·day·atm)) was achieved using 8 bilayers (BL) of electrostatically bonded polyethylenimine (PEI)/polyacrylic acid (PAA).[3] The excellent gas barrier of the PEI/PAA assembly originates from a "scrambled salt" structure, which maximizes the ionic interactions between PEI and PAA. Unfortunately, this ionic bonding network also severely restricts the mobility of polymer chain segments,[30] making PEI/PAA too stiff to be used as a stretchy gas barrier.[3, 31] Replacing PEI with polyethylene oxide (PEO) was found to generate a lower strength hydrogen bonding network that imparts elastomeric behavior to the PAA/PEO multilayer thin films.[30] More recently, a 20 BL PAA/PEO assembly (367 nm thick) was shown to retain a 5X reduction in oxygen transmission rate relative to a bare 1.58 mm natural rubber substrate, even after 100 % strain.[32] The greater openness of this hydrogen-bonded network reduced its gas barrier relative to its electrostatically-bonded counterpart. In the present study, oxygen permeability of PAA/PEO thin films is shown to be tailorable by varying assembling pH. It is found that the permeability first decreases (pH< 2.75) and then increases (pH> 2.75) with increasing pH. PAA/PEO thin films assembled at pH 2.75 exhibit the lowest permeability due to suppressed COOH dimerization and acid ionization, leading to the establishment of the greatest number of intermolecular hydrogen bonds between PAA and PEO. This preferential bonding between H-bond donor and H-bond acceptor also leads to a more homogeneous morphology with smaller dispersed PEO domains. Moreover, the fundamental knowledge about bonding preference, phase morphology and gas barrier of PAA/PEO assemblies provides an understanding of the structure-property relationships in hydrogen-bonded assemblies. The ability to

tailor gas permeability by altering assembling pH could prove very valuable for applications requiring gas barrier (or even separation) in conjunction with elastomeric substrates (e.g., polyisoprene, polyurethane, polybutadiene, etc).

2. Experimental

2.1. Materials

Branched polyethylenimine (M_w = 25,000 g/mol), polyacrylic acid (M_w = 100,000 g/mol), and n-propanol were purchased from Sigma-Aldrich (Milwaukee, WI). Polyethylene oxide (M_w = 4,000,000 g/mol) was purchased from Polysciences (Warrington, PA). All solutions were prepared by rolling for 24 h to achieve equilibrium dissolution. Prior to deposition, the pH of each PEO solution (0.1 wt%), PAA solution (0.1 wt%), and 18 mΩ deionized (DI) rinsing water was altered to the same specified value using 1 M HCl.

2.2. Substrates

Natural rubber film, with a thickness of 1.58 mm, was purchased from McMaster-Carr and used for oxygen transmission rate testing. The rubber was rinsed with DI water, soaked in n-propanol at 40 °C for 10 min, and rinsed again with n-propanol and DI water before being dried with compressed air. Cleaned natural rubber was then treated with an ATTO plasma cleaner (Diener, Germany) at 25 W for 5 min prior to deposition. Polished silicon wafers were used as substrates for ellipsometry and profilometry. Silicon wafers were cut to 10 × 1 cm strips and then cleaned with piranha solution for 30 min, then rinsed with acetone and DI water prior to deposition. *Caution! Piranha solution reacts violently with organic materials and needs to be handled properly.* Polypropylene sheets were used as substrates for making free-standing films that were used for DSC and FTIR testing. Polypropylene sheets were cut to 10 × 3 cm strips, then rinsed with methanol and DI water before deposition. Polished Ti/Au crystals, with a resonance frequency of 5 MHz, were purchased from Maxtek (Cypress, CA) and used to monitor mass deposition using a QCM.

2.3 Layer-by-layer deposition

All cleaned substrates were initially dipped into a 0.1 wt% PEI solution (unaltered pH ~ 10.5) for 10 min and then rinsed with DI water to generate a primer layer. Substrates were then dipped in the PAA solution for 5 min, rinsed with DI water of the same pH three times (20 sec each time), and dried with filtered air. This procedure was followed by an identical dipping, rinsing, and drying procedure in the PEO solution. After this initial bilayer was deposited, additional layers were added using 1 min dipping, with the same rinsing and drying conditions. This procedure was repeated until the desired number of layers was achieved. All thin films were prepared using a home-built robotic dipping system.[33]

2.4 Film characterization

Film thickness was measured (on silicon wafers) using an alpha-SE ellipsometer (J.A. Woollam Co., Inc., Lincoln, NE). Films that were too hazy for the ellipsometer were measured with a P-6 profilometer (KLA-Tencor, Milpitas, CA). Regardless of the measurement method used, reported film thickness was the average of three measurements. Mass of these multilayer films were measured at each layer with a quartz crystal microbalance [QCM] (Inficon, East Syracuse, NY) having a frequency range of 3.8-6 MHz. QCM crystals were cleaned in a PDC-32G plasma cleaner (Harrick Plasma, Ithaca, NY) for 5 min at 10.5 W prior to deposition, then

inserted in a holder and dipped into the corresponding solutions. After each deposition, the crystal was rinsed and dried using the same parameters described above and left on the microbalance to stabilize for 5 min. The reported film mass was the average of the last five data points obtained at the end of 5 min measurement. Thermal property of samples was measured by a Q20 differential scanning calorimeter [DSC] (TA Instruments, New Castle, DE). 5-10 mg of PAA/PEO free-standing film was placed in aluminum pans and scanned from -40 to 80 °C at a heating and cooling rate of 5 °C/min. Oxygen transmission rate measurements were performed by MOCON (Minneapolis, MN) using an Oxtran 2/21 ML oxygen permeability instrument (in accordance with ASTM Standard D-3985) at 23 °C and at 0% RH. 100 BL PAA/PEO thin films assembled at different pH were tested using attenuated total reflection Fourier transform infrared [FTIR] spectroscopy (Bruker Alpha, Billerica, MA), with air taken as the background. All samples were dried at 120 °C under nitrogen atmosphere for 2 hours before being tested. Scan resolution was 2 cm^{-1} and a minimum of 64 scans were signal averaged for each sample. OriginPro software was used to model the summation of two Gaussian peaks.

3. Results and discussion

3.1. Multilayer film growth

Layer-by-layer assembly of PAA/PEO thin films is driven by hydrogen bonding between carboxylic acid groups of PAA (as H-bond donors) and ether groups of PEO (as H-bond acceptors).[34] Although the ability of PEO to act as a hydrogen bond acceptor is unaffected by solution pH due to its non-ionic nature, the capability of PAA to act as hydrogen bond donor is highly dependent on assembling pH.[24, 35] As shown in Fig. 1, with only 5% of COOH groups charged at pH 3.5,[36] the repulsive force between COO$^-$ groups is large enough to prevent the growth of the PAA/PEO assembly.[34] Decreasing assembling pH leads to greater film thickness, due to protonation of COO$^-$ groups, which reduces the intensity of the repulsive force and provides more H-bond donor sites. The influence of pH on film thickness becomes negligible at pH ≤ 2.5 due to complete protonation of carboxylic acid groups on PAA. At pH between 2.5 and 3.5 there is a modulation window,[34] in which PAA is partially ionized.
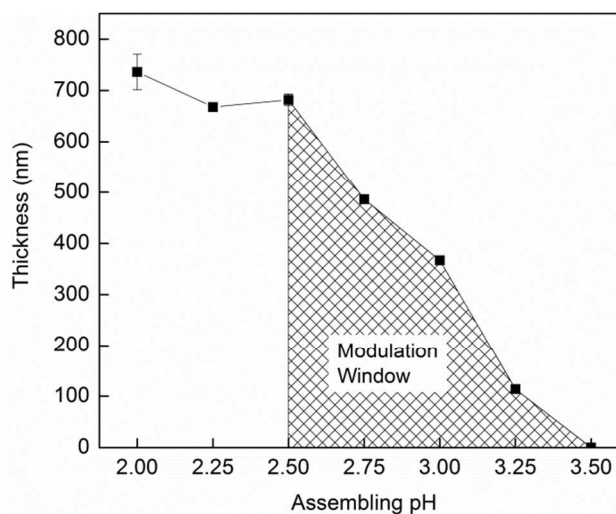
Figure 1. Thickness of 20-bilayer PAA/PEO thin films as a function of assembling pH.

3.2. Intermolecular interactions and thin film composition

Poly(acrylic acid) can form either intramolecular hydrogen bonds with itself, through COOH dimerization, or form intermolecular H-bonds with PEO.[30] The ratio of intra- to inter molecular bond can be quantified using FTIR. The two absorption peaks located at ~1710 and ~1740 cm^{-1} correspond to COOH groups bonded by intra- and intermolecular hydrogen bonds, respectively.[37] As can be qualitatively observed in Fig. 2a, the peak corresponding to intermolecular bonded COOH at 1733 cm^{-1} grows at the expense of the other peak located at 1705 cm^{-1}, indicating more PAA bonds with PEO as pH increases. Spectral deconvolution of all samples is provided in Supporting Information (Fig. S1). The percentage of intermolecular H-bonded COOH was calculated using the method developed by Coleman: intramolecular H-bonded COOH = (area$_{1705}$/(area$_{1705}$/a$_r$ + area$_{1733}$)).[38] The absorptivity ratio (a$_r$) was assumed to be 1.6.[39] As can be seen in Fig. 2b, the percentage of intermolecular hydrogen bonding increases with pH (from 2 to 3), which agrees well with previous findings.[30, 40]
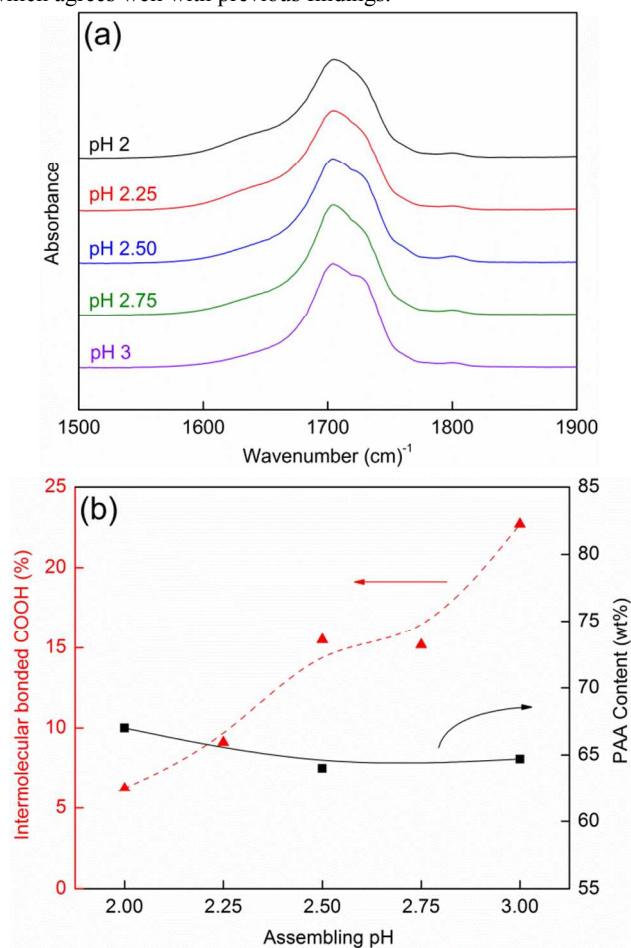
Figure 2. FTIR spectra of the COOH region of PAA/PEO multilayer thin films assembled at varying pH (a). Percentage of intramolecular-bonded COOH [triangles], and PAA content [squares] in the film, as a function of pH (b). [Lines were added to guide the eye]

It is interesting to note that the remarkable change in PAA bonding preference does not alter film composition, as proposed in other studies. In fact, according to quartz crystal microbalance (QCM) measurements, PAA content remains around 65 wt% over the entire pH range (Fig. 2b). This result differs from the findings of previous studies, which suggested that PAA content increased with decreasing pH.[30, 39] According to the proposed hypothesis in these earlier

studies, PAA's tendency to bond with itself at lower pH reduces its ability to bond with PEO. Consequently, more PAA was incorporated into the thin film assembly to bond with PEO (to offset its low bonding efficiency), leading to increased PAA content. It should be noted that although elemental analysis and thermogravimetric analysis were used to confirm this concept, the results were inconclusive.[30, 39] This inability of the old hypothesis to explain the constant content of PAA at different pH provides motivation to propose a new model that describes internal structure and intermolecular interactions of the PAA/PEO assemblies, which are closely related to the oxygen permeability of these multilayer thin films.

3.3. Thin film crystallinity

Fig. 3 shows the second heating scan for 100 BL freestanding PAA/PEO films cycled between -40 and 80 ^{o}C. A single glass transition temperature can be observed for all samples, indicating a macroscopically homogeneous structure within the assembly. A high-temperature melting peak around 66.2 ^{o}C can be observed in all samples (associated with PEO). An additional low-temperature melting peak around 51.5 ^{o}C appears in samples assembled at higher pH (2.75 and 3). This low temperature peak grows at the expense of the high-temperature melting peak with increasing pH. Variation in the melting peak of PEO is believed to originate from microscopic phase separation within the macroscopically homogeneous PAA/PEO assembly.[41] The emergence of a low-temperature melting peak corresponds to thinner crystals that formed in smaller PEO domains. Based on this finding, it is assumed that the size of PEO domains become smaller at higher pH.
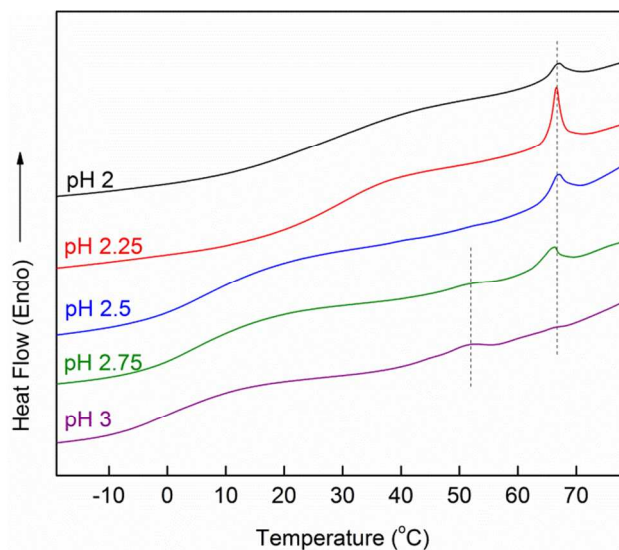
Figure 3. Heating curves for PAA/PEO free-standing films assembled at varying pH.

Polymer crystallinity plays an important role in gas barrier due to the impermeable nature of most polymer crystals, and PEO is known to be semi-crystalline in hydrogen-bonded multilayer assemblies.[41] It is for these reasons that the crystallinity of PEO within PAA/PEO multilayer assemblies is analyzed. The enthalpy of melting for each sample was calculated using the heating curves shown in Fig. 3. The crystallinity (X$_c$) of PEO is calculated based on the following equation:

$$X_c(\%) = \frac{\Delta H}{\Delta H^o \times \Phi} \times 100\%$$

where ΔH is the enthalpy of melting of PEO in the LbL film and $\Delta H°$ is enthalpy of melting of 100% crystalline PEO (188 J/g).[42] Assuming the weight fraction (Φ) of PEO is 35 wt% within the assembly (according to QCM results shown in Fig. 2b), the crystallinity of PEO within the assembly ranges between 1 and 2 %, as shown in Fig. 4. It should be noted that the crystallinity of PEO in PAA/PEO assemblies is smaller than that in PMAA/PEO assemblies (6.2-21.7%).[41] This higher crystallinity may originate from the higher tendency of PMAA to form COOH dimer than PAA, thus leaving more unbonded PEO to crystallize.
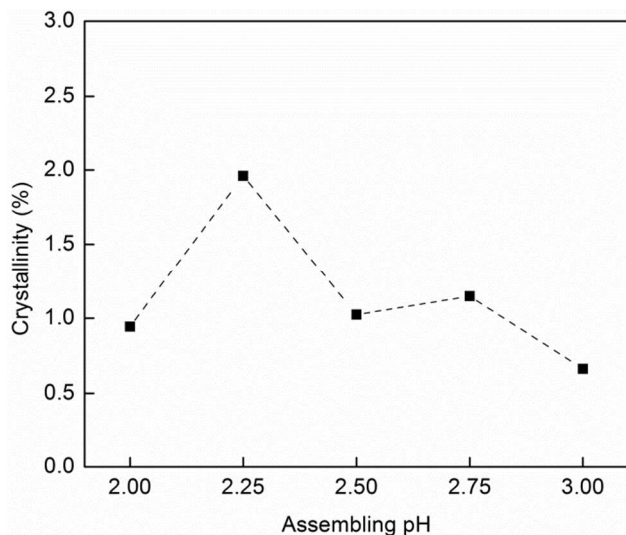
Figure 4. Crystallinity of PEO component in 100 BL PAA/PEO free-standing films assembled at varying pH.

3.4. Gas barrier of hydrogen-bonded assemblies

Changes in intermolecular interaction and phase morphology with varying pH have a direct impact on the oxygen permeability of 20 BL PAA/PEO assemblies, as can be seen in Fig. 5. Film permeability was decoupled from the total permeability using a previously described method.[43] PAA/PEO thin films with the highest oxygen permeability are obtained at pH 2 and 2.25. A slight decrease in permeability can be seen for the film assembled at pH 2.5. The lowest oxygen permeability can be achieved by setting the assembling pH at 2.75, while further increasing the assembling pH to 3 increases permeability. A 50% reduction in oxygen permeability (from 8.1 to 4.1 x10^{-5} cm^3·m/(m^2·day·atm)) is achieved by changing the assembling pH from 2.25 to 2.75. This lowest permeability value is 5 orders of magnitude better than that of natural rubber (1.32 cm^3·m/(m^2·day·atm)). A similar trend can be observed in oxygen transmission rate (OTR) of PAA/PEO coated natural rubber films. A natural rubber plaque coated with 20 PAA/PEO bilayers also exhibits the lowest OTR (40.3 cm^3/(m^2·day·atm)), which is 20X smaller than that of the rubber substrate (840.1 cm^3/(m^2·day·atm)).
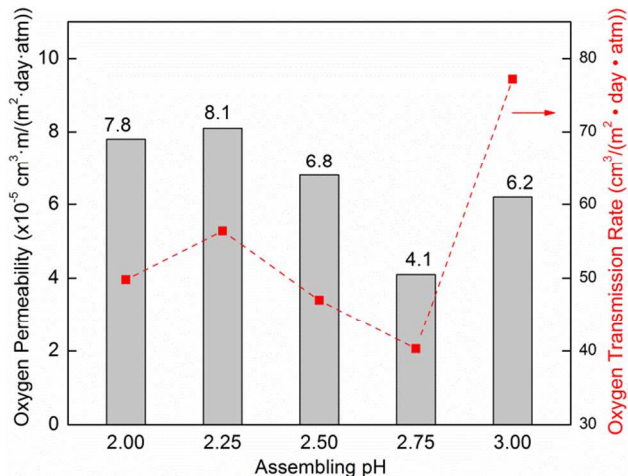
Figure 5. Oxygen permeability [bars] and oxygen transmission rate [squares] of 20 bilayer PAA/PEO thin films assembled at varying pH.

3.5. PAA/PEO structure-property analysis

Gas barrier of all-polymer LbL assemblies depends on several factors. One of the most important of these factors is crystallinity. Neat PEO is a semicrystalline material whose crystallinity can be as high as 77%.[44] Crystallinity is significantly suppressed in the PAA/PEO assembly, due to interdiffusion of polymer chains.[45] Knowing that PEO makes up only 35 wt% of the assembly, the overall crystallinity of PAA/PEO films is around 0.5%, which is too low to have a noticeable influence on oxygen permeability. Consequently, PAA/PEO thin films are treated as amorphous assemblies to simplify the following discussion.

In amorphous polymeric materials, gas barrier is highly dependent on intermolecular interactions.[3, 46-48] As reflected in the growth of PAA/PEO (Fig. 1), formation of hydrogen bonds between PAA and PEO is partly suppressed due to partial ionization of PAA between pH 2.5 and 3.5, leading to thinner multilayer assemblies. As pH decreases within this range, more intermolecular H-bonding is established between these two polymers, which results in lower permeability when the assembling pH decreases from 3 to 2.75.

Besides degree of ionization, the bonding preference of PAA also plays an important role on the intermolecular interactions. Polyacrylic acid can form either intra- or intermolecular hydrogen bonding, but the intramolecular bonds are not very helpful for improving gas barrier. For example, PAA chains can hydrogen-bond with each other in the neat polymer, but even a relatively thick (2.3 μm) PAA film only exhibits marginally improved gas barrier over a polyethylene substrate.[49] On the other hand, bonding between different polymer components within LbL assemblies is known to improve gas barrier of the thin film whether it is ionic or hydrogen bonding.[3, 32] These bonds act as crosslinks within thin films, preventing gas molecule from pushing aside polymer chains to speed diffusion.[50, 51] This evidence suggests that intermolecular hydrogen bonding between PAA and PEO is more effective at improving gas barrier of the PAA/PEO multilayer assemblies. As pH increases from 2 to 2.75, more intermolecular hydrogen bonding can be established, as shown in Figure 2b, leading to reduced oxygen permeability.

The bonding preference of PAA not only controls oxygen permeability, but also influences the size of dispersed PEO domains. At low pH ($\leq$ 2.5), there are very few intermolecular bonds between PAA and PEO. Consequently, poly(ethylene oxide) chains can exist as larger PEO domains rather than forming a more homogeneous, interpenetrating complex with PAA. Thicker PEO crystals can be

formed within these larger domains, leading to the high-temperature melting peak observed in Fig. 3. Increasing pH above 2.5 leads to more H-bonding between PAA and PEO, which increases interdiffusion of polymer chains and results in smaller PEO domains. Thinner PEO crystals generated in these small PEO phases corresponds to the low-temperature melting peak in Fig. 3.

There is an important relationship between the bonding preference of PAA and the size of PEO domains. Smaller PEO domains can be obtained by enhancing the interaction between the dispersed phase (i.e., PEO) and matrix (i.e., PAA or PAA/PEO complex) with more intermolecular hydrogen bonding.[52-54] With the help of smaller PEO domains, it is easier for PAA to form more intermolecular bonds with PEO at the interfaces. If the total volume of PEO is constant as pH increases, smaller PEO domains will produce more specific interfacial area, which can be used to establish more hydrogen bonds. If the total volume of PEO is reduced as pH increases, more PEO becomes part of the matrix,

where PAA and PEO are homogeneously mixed through interdiffusion. This leads to even more intermolecular bonds within the PAA/PEO assembly. No matter which case is true, smaller PEO domains always create more intermolecular hydrogen bonds between PAA and PEO within the assembly. When taken together, it can be concluded that both smaller PEO phase and more intermolecular hydrogen bonding leads to better gas barrier.

The influence of pH on phase morphology and bonding is summarized schematically in Fig. 6. It can be seen that increasing the assembling pH from low (pH 2) to medium (pH 2.75) leads to more intermolecular hydrogen bonding and smaller PEO domains due to reduced COOH dimer content. Further increasing the assembling pH to 3 results in fewer hydrogen bonds, which is caused by ionization of COOH groups. PAA/PEO multilayer thin films assembled at pH 2.75 feature the most highly H-bond networked structure, because the adverse impacts of both PAA ionization and COOH dimerization are minimized.
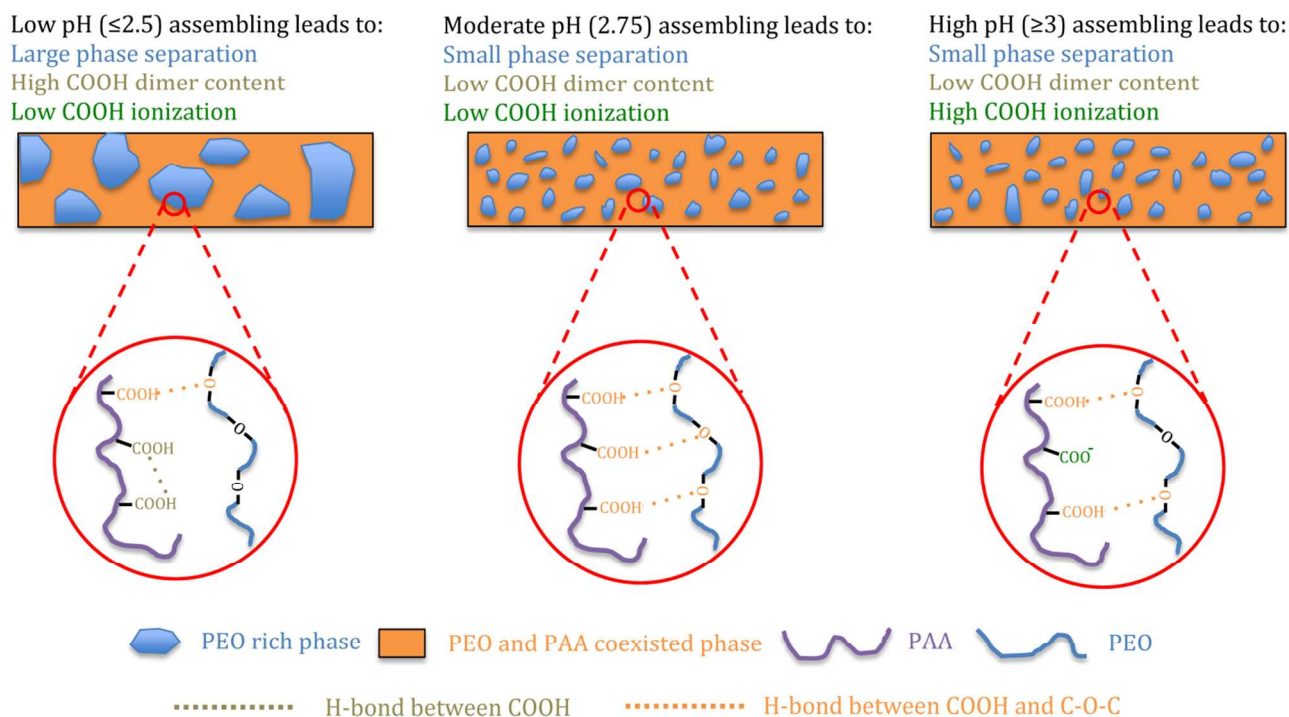
Figure 6. Schematic of internal structures and intermolecular interactions of PAA/PEO assemblies in varying pH regimes.

4. Conclusion

Oxygen permeability of PAA/PEO multilayer thin films was studied as a function of assembling pH. A 50% reduction in oxygen permeability was achieved by adjusting solution pH from 2.25 to 2.75. This reduced permeability was found to be a result of optimized intermolecular interactions. Increasing the assembling pH reduces the COOH dimerization and promotes the formation of intermolecular hydrogen bonding between poly(acrylic acid) and poly(ethylene oxide). Further increasing pH beyond 2.75 leads to excessive ionization that disrupts the formation of intermolecular hydrogen bonds. Although the composition of the PAA/PEO assembly remained the same over the entire pH range (from 2 to 3), smaller PEO domains were obtained at pH 2.75 and 3, which formed thinner crystals (as evidenced by a low-temperature melting peak). The size of

PEO domains is linked to the extent of intermolecular bonding. Smaller PEO domains and greater intermolecular hydrogen bonding simultaneously contribute to better gas barrier. Assembling multilayer films at pH 2.75 will minimize the negative impacts of PAA ionization, COOH dimerization, and phase separation, leading to the lowest oxygen permeability. This unique combination of gas barrier, with previously established stretchability,[30, 32] makes these thin films very useful for imparting protection to elastomeric substrates (e.g. tires, bladders, etc.).

Acknowledgement

References

1. T. V. Duncan, *J. Colloid Interface Sci.*, 2011, **363**, 1-24.
2. C. Silvestre, D. Duraccio and S. Cimmino, *Prog. Polym. Sci.*, 2011, **36**, 1766-1782.
3. Y. H. Yang, M. Haile, Y. T. Park, F. A. Malek and J. C. Grunlan, *Macromolecules*, 2011, **44**, 1450-1459.
4. F. Carosio, S. Colonna, A. Fina, G. Rydzek, J. Hemmerlé, L. Jierry, P. Schaaf and F. Boulmedais, *Chem. Mater.*, 2014, **26**, 5459-5466.
5. J. S. Lewis and M. S. Weaver, *IEEE J. Quant. Electron.*, 2004, **10**, 45-57.
6. B. Stevens, E. Dessiatova, D. A. Hagen, A. D. Todd, C. W. Bielawski and J. C. Grunlan, *ACS Appl. Mater. Interfaces*, 2014, **6**, 9942-9945.
7. M.-C. Choi, Y. Kim and C.-S. Ha, *Prog. Polym. Sci.*, 2008, **33**, 581-630.
8. K. M. Holder, B. R. Spears, M. E. Huff, M. A. Priolo, E. Harth and J. C. Grunlan, *Macromol. Rapid Commun.*, 2014, **35**, 960-964.
9. M. Bhattacharya, S. Biswas and A. K. Bhowmick, *Polymer*, 2011, **52**, 1562-1576.
10. S. Takahashi, H. A. Goldberg, C. A. Feeney, D. P. Karim, M. Farrell, K. O'Leary and D. R. Paul, *Polymer*, 2006, **47**, 3083-3093.
11. A. J. Svagan, A. Åkesson, M. Cárdenas, S. Bulut, J. C. Knudsen, J. Risbo and D. Plackett, *Biomacromolecules*, 2012, **13**, 397-405.
12. H. Wang, J. K. Keum, A. Hiltner, E. Baer, B. Freeman, A. Rozanski and A. Galeski, *Science*, 2009, **323**, 757-760.
13. M. Frounchi, S. Dadbin, Z. Salehpour and M. Noferesti, *J. Membr. Sci.*, 2006, **282**, 142-148.
14. H. Kim, Y. Miura and C. W. Macosko, *Chem. Mater.*, 2010, **22**, 3441-3450.
15. M. W. Möller, T. Lunkenbein, H. Kalo, M. Schieder, D. A. Kunz and J. Breu, *Adv. Mater.*, 2010, **22**, 5245-5249.
16. J. M. Herrera-Alonso, Z. Sedlakova and E. Marand, *J. Membr. Sci.*, 2010, **349**, 251-257.
17. K. Zeng and Y. Bai, *Mater. Lett.*, 2005, **59**, 3348-3351.
18. E. Picard, H. Gauthier, J. F. Gerard and E. Espuche, *J. Colloid Interface Sci.*, 2007, **307**, 364-376.
19. P. Podsiadlo, A. K. Kaushik, E. M. Arruda, A. M. Waas, B. S. Shim, J. Xu, H. Nandivada, B. G. Pumplin, J. Lahann, A. Ramamoorthy and N. A. Kotov, *Science*, 2007, **318**, 80-83.
20. M. A. Priolo, D. Gamboa, K. M. Holder and J. C. Grunlan, *Nano Lett.*, 2010, **10**, 4970-4974.
21. Y.-H. Yang, L. Bolling, M. A. Priolo and J. C. Grunlan, *Adv. Mater.*, 2013, **25**, 503-508.
22. G. Decher and J.-D. Hong, *Makromol. Chem. Macromol. Symp.*, 1991, **46**, 321-327.
23. G. Decher, *Science*, 1997, **277**, 1232-1237.
24. S. A. Sukhishvili and S. Granick, *Macromolecules*, 2002, **35**, 301-310.
25. M. A. Priolo, D. Gamboa and J. C. Grunlan, *ACS Appl. Mater. Interfaces*, 2010, **2**, 312-320.
26. M. A. Priolo, K. M. Holder, D. Gamboa and J. C. Grunlan, *Langmuir*, 2011, **27**, 12106-12114.
27. F. Xiang, P. Tzeng, J. S. Sawyer, O. Regev and J. C. Grunlan, *ACS Appl. Mater. Interfaces*, 2013, **6**, 6040-6048.
28. M. A. Priolo, K. M. Holder, S. M. Greenlee, B. E. Stevens and J. C. Grunlan, *Chem. Mater.*, 2013, **25**, 1649-1655.
29. M. A. Priolo, K. M. Holder, S. M. Greenlee and J. C. Grunlan, *ACS Appl. Mater. Interfaces*, 2012, **4**, 5529-5533.
30. J. L. Lutkenhaus, K. D. Hrabak, K. McEnnis and P. T. Hammond, *J. Am. Chem. Soc.*, 2005, **127**, 17228-17234.
31. D. Kim, P. Tzeng, K. J. Barnett, Y.-H. Yang, B. A. Wilhite and J. C. Grunlan, *Adv. Mater.*, 2014, **26**, 746-751.
32. F. Xiang, S. M. Ward, T. M. Givens and J. C. Grunlan, *ACS Macro Lett.*, 2014, 1055-1058.
33. W. S. Jang and J. C. Grunlan, *Rev. Sci. Instrum.*, 2005, **76**.
34. D. M. DeLongchamp and P. T. Hammond, *Langmuir*, 2004, **20**, 5403-5411.
35. E. Kharlampieva and S. A. Sukhishvili, *J. Macromol. Sci. Polymer. Rev.*, 2006, **46**, 377-395.
36. K. L. Smith, A. E. Winslow and D. E. Petersen, *Ind. Eng. Chem.*, 1959, **51**, 1361-1364.
37. M. M. Coleman, J. Y. Lee, C. J. Serman, Z. Wang and P. C. Painter, *Polymer*, 1989, **30**, 1298-1307.
38. J. Y. Lee, P. C. Painter and M. M. Coleman, *Macromolecules*, 1988, **21**, 346-354.
39. J. L. Lutkenhaus, K. McEnnis and P. T. Hammond, *Macromolecules*, 2007, **40**, 8367-8373.
40. M. M. Coleman and P. C. Painter, *Prog. Polym. Sci.*, 1995, **20**, 1-59.
41. C. Sung, A. Vidyasagar, K. Hearn and J. L. Lutkenhaus, *Langmuir*, 2012, **28**, 8100-8109.
42. S. Cimmino, E. Di Pace, E. Martuscelli and C. Silvestre, *Macromol. Chem. Phys.*, 1990, **191**, 2447-2454.
43. W. S. Jang, I. Rawson and J. C. Grunlan, *Thin Solid Films*, 2008, **516**, 4819-4825.
44. K. K. Maurya, N. Srivastava, S. A. Hashmi and S. Chandra, *J. Mater. Sci.*, 1992, **27**, 6357-6364.
45. E. Kharlampieva, V. Kozlovskaya, J. F. Ankner and S. A. Sukhishvili, *Langmuir*, 2008, **24**, 11346-11349.
46. Z. Zhang, I. J. Britt and M. A. Tung, *J. Appl. Polym. Sci.*, 2001, **82**, 1866-1872.
47. T. H. McHugh and J. M. Krochta, *J. Agric. Food. Chem.*, 1994, **42**, 841-845.
48. N. Gontard, R. Thibault, B. Cuq and S. Guilbert, *J. Agric. Food. Chem.*, 1996, **44**, 1064-1069.
49. L. J. Ward, W. C. E. Schofield, J. P. S. Badyal, A. J. Goodwin and P. J. Merlin, *Chem. Mater.*, 2003, **15**, 1466-1469.
50. J. M. Lagaron, R. Catalá and R. Gavara, *Mater. Sci. Technol.*, 2004, **20**, 1-7.

51. J. J. Kochumalayil and L. A. Berglund, *Green Chemistry*, 2014, **16**, 1904-1910.
52. X. Zhang, K. Takegoshi and K. Hikichi, *Macromolecules*, 1992, **25**, 2336-2340.
53. M. Avella and E. Martuscelli, *Polymer*, 1988, **29**, 1731-1737.
54. E. J. Moskala, S. E. Howe, P. C. Painter and M. M. Coleman, *Macromolecules*, 1984, **17**, 1671-1678.

Notes

[a] Department of Mechanical Engineering, Texas A&M University, College Station, TX 77843-3123, United States.

[b] Department of Chemistry, Texas A&M University, College Station, TX 77842-3012, United States.

[*] Corresponding author. Phone: 979.845.3027, Fax: 979.845.3081, E-mail: jgrunlan@tamu.edu (Jaime C. Grunlan)

Soft Matter Accepted Manuscript

Soft Matter

ARTICLE

For Table of Contents Only

Structural tailoring of hydrogen-bonded poly(acrylic acid)/poly(ethylene oxide) multilayer thin films for reduced gas permeability

Fangming Xiang, Sarah M. Ward, Tara M. Givens and Jaime. C. Grunlan
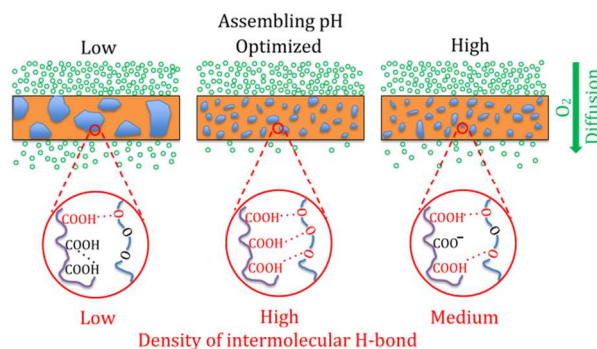
Setting the assembling pH at 2.75 minimizes the negative impacts of poly(acrylic acid) ionization, COOH dimerization, and phase separation on the formation of intermolecular hydrogen bonds within a poly(acrylic acid)/poly(ethylene oxide) assembly, leading to low oxygen permeability.

Soft Matter Accepted Manuscript